

Properties of cage rearrangements observed near the colloidal glass transition

Eric R. Weeks^{*,(1)} and D. A. Weitz⁽²⁾

⁽¹⁾*Physics Department, Emory University, Atlanta, GA 30322*

⁽²⁾*Department of Physics and DEAS, Harvard University, Cambridge, MA 02138*

(July 12, 2001)

Abstract

We use confocal microscopy to study the motions of particles in concentrated colloidal systems. Near the glass transition, diffusive motion is inhibited, as particles spend time trapped in transient “cages” formed by neighboring particles. We measure the cage sizes and lifetimes, which respectively shrink and grow as the glass transition approaches. Cage rearrangements are more prevalent in regions with lower local concentrations and higher disorder. Neighboring rearranging particles typically move in parallel directions, although a nontrivial fraction move in anti-parallel directions.

Typeset using REVTeX

PACS numbers: 61.43.Fs, 64.70.Pf, 82.70.Dd, 61.20.Ne

Many liquids undergo a glass transition when rapidly cooled, where their viscosity grows by orders of magnitude for only modest decreases in temperature. This drastic increase in viscosity is unaccompanied by significant structural changes; instead, the dynamics slow dramatically [1]. Physically, this slowing of the dynamics reflects the confinement of any given particle by a “cage” formed by its neighbors; it is the breakup or rearrangement of the cage which leads to the final structural relaxation, allowing the particle to diffuse through the sample. The dynamics of the cages have been studied with scattering measurements, which probe a spatial and temporal average of their behavior; however, the actual motion of the individual particles involved in cage dynamics and breakup are still very poorly understood [1–7].

In this paper, we study the motion of the individual particles and their neighbors during cage breakup, and provide the first direct visualization and detailed analysis of this process. We use confocal microscopy to study the motion of colloidal particles in a dense suspension, an excellent model for the glass transition [8–11]. We directly probe the nature of the motion during cage rearrangement, finding that the majority of neighboring particles move in the same direction, while a significant minority move in opposite directions, resulting in local changes in topology. We also measure the local environment to search for the physical origins of the motion leading to cage rearrangement, finding that more mobile particles are located in regions with a lower local volume fraction, and higher disorder. These measurements provide a direct, quantitative physical picture of the nature of these rearrangements.

We use sterically stabilized poly-(methylmethacrylate) particles with a radius $a = 1.18 \mu\text{m}$ [3,12,13], immersed in a mixture of decalin and cycloheptylbromide, a solvent that simultaneously matches the particle index of refraction and density; this mitigates the effects of scattering and sedimentation. Hard sphere particles undergo a freezing transition at a volume fraction $\phi_f = 0.494$, a melting transition at $\phi_m = 0.545$, and have a glass transition at $\phi_g \approx 0.58$ [8,11]. To visualize the particles, we stain them with fluorescent rhodamine dye; this imparts a slight charge to the particles, shifting the phase transition boundaries

to $\phi_f \approx 0.38$, $\phi_m \approx 0.42$, and $\phi_g \approx 0.58$. We image a volume $60 \mu\text{m} \times 60 \mu\text{m} \times 10 \mu\text{m}$, containing several thousand particles, and identify particle centers with an accuracy of at least $0.05 \mu\text{m}$ [12,14]. A typical particle trajectory is shown in the inset of Fig. 1; it exhibits caged motion, with a sudden cage rearrangement which lasts ~ 600 s.

The nature of the caging is evident from the particle mean square displacement, $\langle \Delta x^2 \rangle$, shown in Fig. 2(a) for two supercooled colloidal fluids ($\phi < \phi_g$). At the earliest time scales, the particle motion is diffusive, since their displacement is so small that they have not yet encountered the cage formed by their neighbors. As their displacement becomes larger, their motion is impeded by the cage, leading to the plateau in $\langle \Delta x^2 \rangle$. The displacement at the plateau decreases as ϕ increases, reflecting the smaller cage size. Moreover, the cages become more long-lived with increasing ϕ ; this presumably results from the fact that cage rearrangements involve a larger number of particles as the glass transition is approached [2–5]. The cage rearrangement itself leads to the increase in $\langle \Delta x^2 \rangle$ at the end of the plateau; at even longer lag times, the asymptotic motion again becomes diffusive, albeit with a greatly decreased diffusion coefficient, D_∞ , as indicated by the dashed lines in Fig. 2.

We estimate the time scale for cage rearrangement, Δt^* , by finding the maximum of the nongaussian parameter $\alpha_2(\Delta t) = \langle \Delta x^4 \rangle / (3\langle \Delta x^2 \rangle^2) - 1$; α_2 is computed from the 1D displacement distribution function $P(\Delta x; \Delta t)$ [3–5,15], and is zero for a gaussian distribution and largest when there are broad tails in the distribution. Insight into the nature of these rearrangement motions is obtained in Fig. 1 shows a cut through the sample. The rearrangement of cages involves the cooperative motion of several neighboring particles moving in similar directions, as indicated by arrows attached to particles with the largest displacements [2–5]. To quantify the nature of this behavior it is useful to consider the dependence on particle step size $\Delta r / \bar{r}$ at Δt^* , where $\bar{r} \equiv \langle \Delta r^2 \rangle^{1/2}$. We plot the radial step size distribution, $P(\Delta r / \bar{r})$ in Fig. 3(a). There are more large displacements than expected for a gaussian distribution, shown by the dashed line; moreover, as ϕ_g is approached, the tails become even broader, as shown by the circles for $\phi = 0.56$. This reflects the anomalously large motion of the particles undergoing cage rearrangements.

The increase in the mean square displacement at lag times greater than Δt^* is due to an increased motion of at least some of the particles. To confirm that this motion directly reflects structural relaxation, we calculate a topological cage correlation function, $C_{\text{cage}}(\Delta t)$ [6]. We define particles as nearest neighbors if their separation is less than a cutoff distance set by the first minimum of the pair correlation function $g(r)$; $C_{\text{cage}}(\Delta t)$ is the fraction of particles with the same neighbors at time t and time $t + \Delta t$, averaged over all t . As shown in Fig. 2(b), for the lowest volume fraction, $\phi = 0.46$ (triangles), the particles are barely caged. As ϕ increases toward ϕ_g , the decay slows dramatically; moreover, a pronounced change in the decay of the correlation function occurs at Δt^* . To determine which particles are responsible for topological changes, we replot $C_{\text{cage}}(\Delta t^*)$ as a function of the normalized displacement. As shown in Fig. 3(b), $C_{\text{cage}}(\Delta t^*)$ decreases significantly for particles with larger displacements. This confirms that these are the ones that contribute most to the structural relaxation.

To directly measure the size of the cage, we investigate the temporal correlations of the motion of individual particles [7]. All particles move due to Brownian motion. However, those that remain caged must have no significant net displacement over long times; by contrast those whose cages rearrange do have net displacements. To quantify this, we compare a particle's displacements $\Delta\vec{r}$ and $\Delta\vec{r}'$ during sequential time intervals of Δt^* . We focus on x' , the component of $\Delta\vec{r}'$ along the direction of the original displacement $\Delta\vec{r}$; $\langle x' \rangle$ is plotted in Fig. 3(c). The values of $\langle x' \rangle$ are always less than zero, indicating that the average motion is anticorrelated. For small initial displacements the behavior is linear, $x' = -c|\langle \Delta\vec{r} \rangle|$; larger values of c indicate more highly anticorrelated motion. The cage constrains a particle so that the larger distance a particle moves, the greater it will move back. The linear relationship fails for larger displacements, as seen in Fig. 3(c); thus the degree of anticorrelation actually decreases – particles move shorter distances $\langle x' \rangle$ than expected by linear extrapolation from the small $\Delta\vec{r}$ behavior. We identify the end of the linear regime as the cage size, r_{cage} . r_{cage} is relatively insensitive to Δt , showing that the cage size is a time-scale independent quantity [7]. For comparison, we estimate the size of the

cage by other methods. The simplest is based on the free volume of the system compared to random close packing, $r_{\text{est}} = 4a[(\phi_{rcp}/\phi)^{1/3} - 1]$. Another estimate comes from the mean square displacement at the cage rearrangement time scale Δt^* , $r_{\text{msd}} = \langle \Delta r^2(\Delta t^*) \rangle^{1/2}$. The final estimate is $\Delta r^*(\Delta t^*)$, chosen so that 5% of particles have displacements $\Delta r > \Delta r^*$ [3]. The values of all of these estimates are listed in Table 1 and are in good agreement. Thus we are able to obtain a robust measure of the cage size.

We can use our measure of the cage size to determine the number of particles involved in cage rearrangements at any given time. At long times, the diffusive motion reflects particles undergoing many cage rearrangements, each with motion over a distance r_{cage} , in random directions. Thus, we consider the particle motion to be a random walk, alternating between steps (cage rearrangements) and pauses (caging). From the Central Limit Theorem, $D_\infty = r_{\text{cage}}^2/2\Delta t^{**}$, where Δt^{**} is the mean time between steps, or the average lifetime of the cages [16]. The measured values of D_∞ , and the calculated values of Δt^{**} are listed in Table 1. We find that Δt^{**} is significantly larger than Δt^* , the time scale for a particle to move *during* one cage rearrangement; both grow as ϕ increases. While the cage size decreases, it remains finite as ϕ_g is approached, implying that the dramatic decrease in D_∞ is due primarily to the increasing cage lifetime. Our random-walk picture also yields an unambiguous estimate of the fraction of particles involved in cage rearrangements at any given time; it is given by the ratio $\Delta t^*/\Delta t^{**}$. This ratio is $\sim 8\%$ for all samples except the most dilute (for which it is 16%); it is shown by the vertical dashed line in Fig. 3(a).

To search for the underlying origins of the cage rearrangements, we investigate local properties which may drive particle mobility. We compute the Voronoi polyhedra for the particles, and determine the local volume per particle [3]. Locally, the volume per particle fluctuates greatly from particle to particle; however, on average, the particles with larger displacements have larger Voronoi volumes, as shown in Fig. 3(d). The variation in local volume fraction is $\delta\phi = O(0.03)$, which can be quite significant, particularly close to ϕ_g , where small variations in ϕ can cause dramatic changes in behavior. After the particles have moved, their Voronoi volume is generally closer to the average. These results suggest that

the particles with smaller ϕ are farther from ϕ_g and thus are more likely to rearrange.

Ultimately, the sample will crystallize, and it is therefore possible that the evolution to crystalline order drives the structural relaxation. To investigate this possibility, we quantify the local order with an order parameter that identifies local crystalline regions from particle positions [17,18]. If two adjacent particles have similar orientations of their neighbors about each of them, the two particles are ordered neighbors. The average number of ordered neighbors for each particle is between 2 and 4, with particles with larger displacements having fewer ordered neighbors, as shown in Fig. 3(e); furthermore, these particles typically move to positions where their number of ordered neighbors has increased by ~ 1 . This suggests that there is a slow evolution toward crystalline structure. We emphasize, however, that crystallization occurs on time scales significantly longer than these observations; moreover, crystallization is a nucleation and growth process, with full crystalline order of the sample resulting from the growth of only a small number of nuclei. Thus, any effect of the local crystal order on the cage rearrangement may be driven more by local variations in volume fraction, rather than an evolution to the state with the lowest global energy minimum [18].

Cage rearrangement is not strictly a localized event; instead, a typical structural relaxation can involve many neighboring particles, which often move in similar directions, as shown by the arrows in Fig. 1 [2–5]. To quantify the propensity for motion of neighboring particles in the same direction, we calculate the distribution of angles, $P(\theta)$, between the displacement vectors of all neighboring particles, measured at Δt^* to define the displacements. The probability of observing two displacement vectors forming an angle in the range $(\theta, \theta + d\theta; \phi, \phi + d\phi)$ is given by $P(\theta, \phi) \sin \theta d\theta d\phi$; in Fig. 4(a) we plot $P(\theta, \phi)$ which, by symmetry, depends only on θ . This function is strongly peaked at $\theta \approx 0$, indicating that two particles usually move in parallel directions (“strings”) [5], although a significant fraction of particles move in anti-parallel directions ($\theta \approx \pi$, “mixing regions”). The distribution $P(\theta, \phi)$ remains qualitatively unchanged even considering only pairs of particles with large displacements, which are involved in cage rearrangements. When $\theta \approx \pi$ particles are either moving toward each other or away from each other; examples of each case can be seen in

Fig. 1. We find that these “mixing” pairs of particles ($\theta > \pi/2$) are approximately twice as likely to result in the two particles no longer being neighbors (compared to the pairs with $\theta < \pi/2$). Thus, these rearrangements, while less frequent, are responsible for much of the topological changes.

To investigate the nature of the correlation of the motion between neighboring particles, we calculate the probability distribution function, $P(\Delta R_{12}|R_{12})$, which measures the change in separation, ΔR_{12} , between two nearby particles, initially separated a distance, R_{12} , after an elapsed time interval of Δt^* . The width of a typical distribution is much more narrow for initial separations at peaks of the pair correlation function, $g(R_{12})$, than those that at minima, as shown by the solid and dashed lines in the insert of Fig. 4(b), which correspond respectively to the first peak and the first minimum in $g(R_{12})$. This is shown more dramatically in Fig. 4(b), where we compare the widths of the distribution functions, $\sigma_{R_{12}}$, directly with $g(R_{12})$; there is clear correlation between the peaks in the pair correlation function and the dips in the width of the distribution. This correlation is reminiscent of the behavior of the collective diffusion coefficient, which varies as the inverse of the static structure factor, $D(q) \sim 1/S(q)$ [19]. The relaxation of fluctuations at the peak of the structure factor, which reflects the most favorable structure, is slowed relative to other values of q . A similar behavior occurs in real space; particles whose separation corresponds to a peak in $g(R_{12})$ are in more favorable relative positions and tend to move together, so that their separation does not change; by contrast, particles whose separation corresponds to a minimum in $g(R_{12})$ are in less favorable relative positions, and tend to move in antiparallel directions.

The symmetry of the distribution shown by the dashed line in Fig. 4(b) suggests that converging and diverging pairs of particles occur with equal probability. In fact, we examined several individual cases of particles moving in anti-parallel directions and find that typically these involve *four* particles: the particles start in a diamond pattern around a small void, with two particles moving in (to become nearest neighbors) while the other two move outward to make room (becoming second-nearest neighbors). This suggests a broad interpretation of the cooperativity of cage rearrangements, ranging from “string-like” cooperative motion

to anti-parallel movements.

This work reveals a physical picture of cage-trapping and rearrangement. Cage rearrangements involve localized clusters of particles with large displacements, in regions with higher disorder and higher free volume. Rearranging particles often move in parallel directions (string-like motion). However, there are also “mixing regions” where a smaller fraction of particles move in other directions [Fig. 4(a)]; this motion accounts for a significant fraction of the topological rearrangements within supercooled fluids. Both the collective nature of the relaxation, and the local origin of the cage rearrangements, are not incorporated in theories of the glass transition. They clearly play a key role in the behavior of supercooled fluids of colloidal suspensions; it remains to be seen whether they also are important effects in other glasses.

We thank J. Conrad, J. C. Crocker, B. Doliwa, U. Gasser, S. C. Glotzer, H. Gould, and K. Vollmayr-Lee for helpful discussions. We thank A. Schofield for providing our colloidal samples. This work was supported by NSF (DMR-9971432) and NASA (NAG3-2284).

REFERENCES

* Electronic mail: weeks@physics.emory.edu

- [1] C. A. Angell, *Science* **267**, 1924 (1995); F. H. Stillinger, *ibid.* **267**, 1935 (1995); M. D. Ediger, C. A. Angell, S. R. Nagel, *J. Phys. Chem.* **100**, 13200 (1996); C. A. Angell, *J. Phys. Cond. Mat.* **12**, 6463 (2000).
- [2] W. K. Kegel and A. van Blaaderen, *Science* **387**, 290 (2000).
- [3] E. R. Weeks, J. C. Crocker, A. C. Levitt, A. Schofield, and D. A. Weitz, *Science* **287**, 627 (2000).
- [4] W. Kob, C. Donati, S. J. Plimpton, P. H. Poole, S. C. Glotzer, *Phys. Rev. Lett.* **79**, 2827 (1997).
- [5] C. Donati et al., *Phys. Rev. Lett.* **80**, 2338 (1998).
- [6] E. Rabani, J. D. Gezelter, and B. J. Berne, *J. Chem. Phys.* **107**, 6867 (1997).
- [7] B. Doliwa and A. Heuer, *Phys. Rev. Lett.* **80**, 4915 (1998).
- [8] P. N. Pusey and W. van Megen, *Nature* **320**, 340 (1986).
- [9] E. Bartsch, V. Frenz, S. Möller, H. Silesco, *Physica A* **201**, 363 (1993).
- [10] W. van Megen and S. M. Underwood, *Phys. Rev. E* **49**, 4206 (1994).
- [11] W. van Megen, T. C. Mortensen, S. R. Williams, J. Müller, *Phys. Rev. E* **58**, 6073 (1998).
- [12] A. D. Dinsmore, E. R. Weeks, V. Prasad, A. C. Levitt, D. A. Weitz, to be published in *App. Opt.* (2001).
- [13] L. Antl et. al., *Colloids and Surfaces* **17**, 67 (1986).
- [14] J. C. Crocker and D. G. Grier, *J. Colloid Interface Sci.* **179**, 298 (1996).

- [15] A. Rahman, Phys. Rev. **136**, A405 (1964).
- [16] E. R. Weeks and H. L. Swinney, Phys. Rev. E **57**, 4915 (1998); J. P. Bouchaud and A. Georges, Phys. Rep. **195**, 127 (1990).
- [17] P. Rein ten Wolde, M. J. Ruiz-Montero, D. Frenkel, J. Chem. Phys. **104**, 9932 (1996).
- [18] U. Gasser, E. R. Weeks, A. Schofield, D. A. Weitz, Science **292**, 258 (2001).
- [19] P. N. Pusey, in *Liquids, Freezing and the Glass Transition*, edited by J. P. Hansen, D. Levesque, and J. Zinn-Justin (Elsevier, Amsterdam, 1991), Chap. 10.

TABLES

TABLE I. Estimates for the cage size, the cage rearrangement time scale Δt^* , the cage lifetime Δt^{**} , and the asymptotic diffusion coefficient D_∞ .

ϕ	cage size (μm)				time scales (hr)		D_∞ ($\mu\text{m}^2/\text{s}$)
	r_{cage}	r_{est}	r_{msd}	Δr^*	Δt^*	Δt^{**}	
0.46	0.75	0.55	0.63	1.12	0.083	0.52	$15 \cdot 10^{-5}$
0.52	0.35	0.35	0.23	0.40	0.17	2.1	$0.80 \cdot 10^{-5}$
0.53	0.45	0.31	0.27	0.49	0.67	9.4	$0.30 \cdot 10^{-5}$
0.56	0.25	0.21	0.17	0.29	0.28	3.3	$0.26 \cdot 10^{-5}$

FIGURES

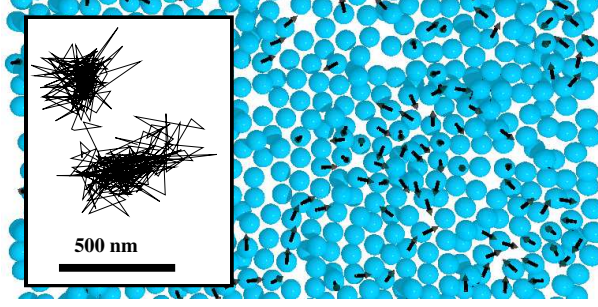


FIG. 1. Cut through the middle of a three-dimensional sample, with arrows indicating the direction of motion for particles with displacements $\Delta r > 0.2 \mu\text{m}$, using $\Delta t^* = 600 \text{ s}$. The sample has $\phi = 0.52$, and the cut is $2.5 \mu\text{m}$ thick (~ 1 layer of particles). The arrows are all the same length, so shortened arrows indicate motion in or out of the picture. Inset: 120 min trajectory of one particle from this sample.

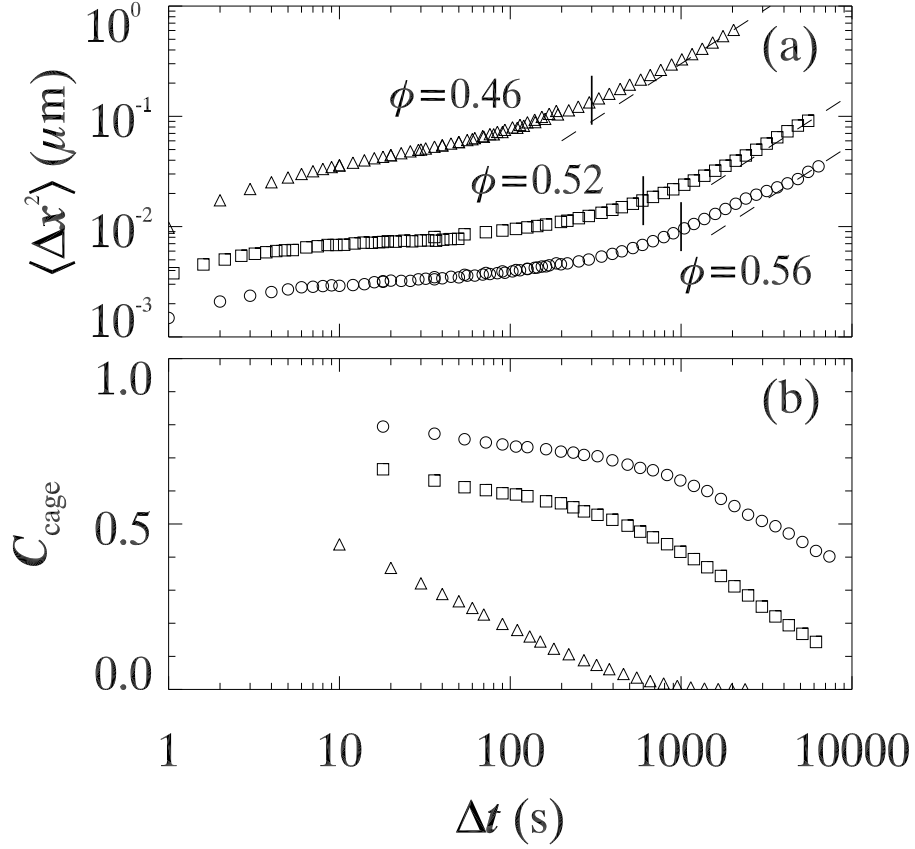


FIG. 2. (a) Mean square displacements. The diagonal straight lines indicate estimates for D_∞ . Vertical bars indicate Δt^* . (b) The cage correlation function.

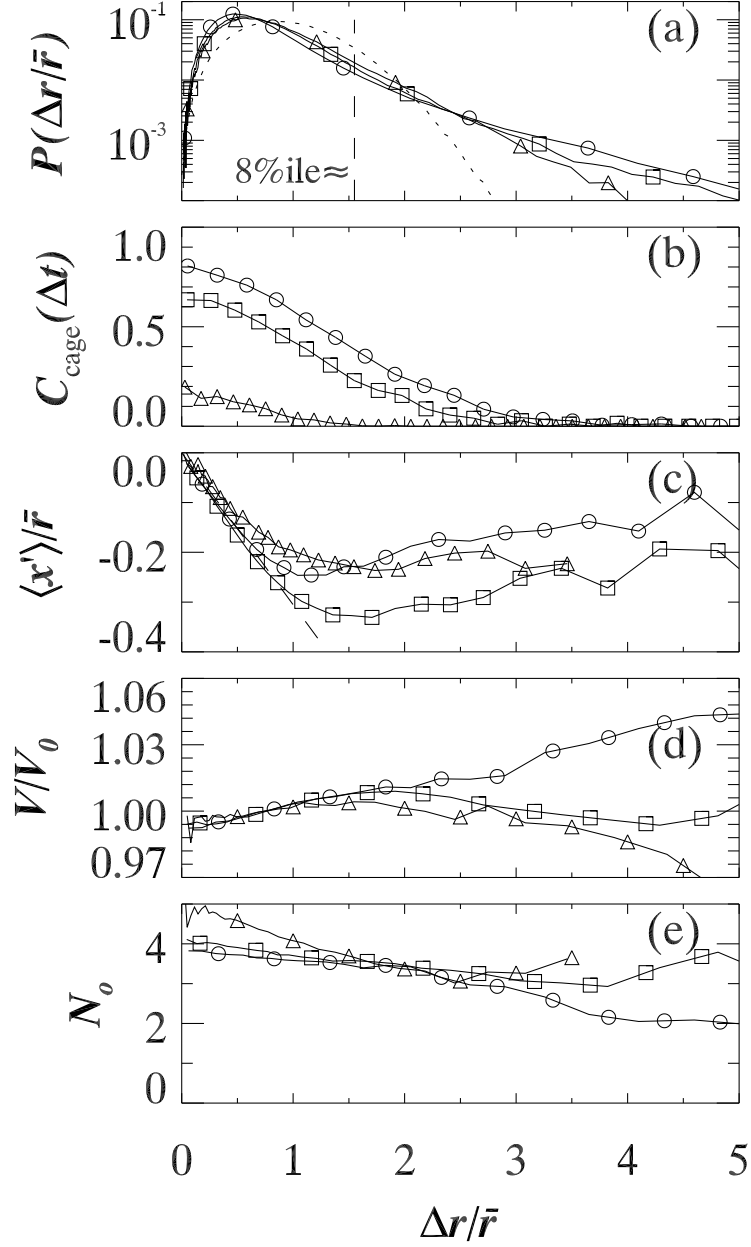


FIG. 3. (a) Step-size distribution. The vertical dashed line indicates the 8%ile cutoff. The dotted line is a gaussian with width $\bar{r} = 1$. (b) $C_{\text{cage}}(\Delta t^*; \Delta r)$. (c) Average subsequent displacement $\langle x' \rangle$ along the direction of the original displacement Δr . The dashed line is a linear fit to the small Δr region for the $\phi = 0.56$ data (circles). (d) The average Voronoi volume per particle V , normalized by the sample average V_0 . (e) The average number of ordered neighbors N_o particles have. The symbols are: triangles $\phi = 0.46$, $\Delta t^* = 300$ s, $\bar{r} = 0.61$ μm ; squares $\phi = 0.52$, $\Delta t^* = 600$ s, $\bar{r} = 0.22$ μm ; circles $\phi = 0.56$, $\Delta t^* = 1000$ s, $\bar{r} = 0.16$ μm .

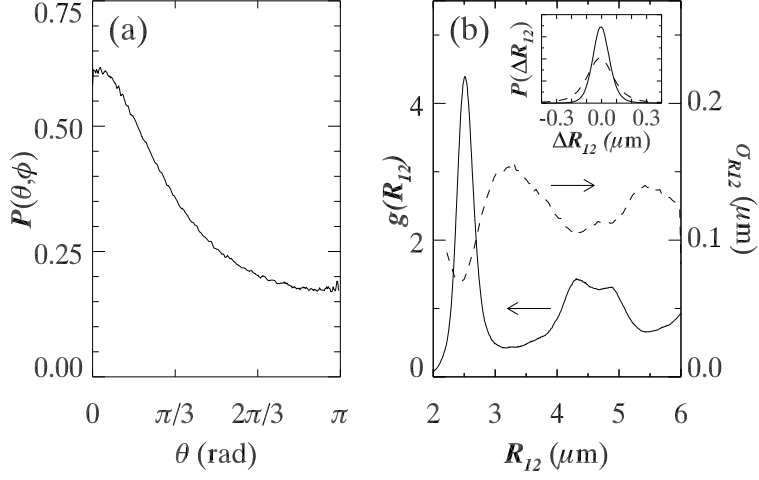


FIG. 4. (a) Probability distribution of angle between displacement vectors for two neighboring particles, as a function of the polar angle θ . (b) Pair correlation function $g(R_{12})$ (solid line) and width $\sigma_{R_{12}}$ of probability distribution function $P(\Delta R_{12}|R_{12})$ (dashed line). Insert shows $P(\Delta R_{12}|R_{12})$ for nearest neighbors, with initial separations of $2.4 \mu\text{m} < R_{12} < 2.6 \mu\text{m}$ (solid line), and anti-neighbors with $3.0 \mu\text{m} < R_{12} < 3.2 \mu\text{m}$ (dotted line). All data are for $\phi = 0.56$ and $\Delta t^* = 1000s$.